

Clustering of gold atoms in ion-implanted silica after thermal annealing in different atmospheres

A. Miotello

INFN-Dipartimento di Fisica, Università di Trento, I-38050 Povo, Trento, Italy

G. De Marchi, G. Mattei,* P. Mazzoldi, and C. Sada

INFN-Dipartimento di Fisica, Università di Padova, via Marzolo 8, I-35131 Padova, Italy

(Received 2 May 2000; revised manuscript received 29 August 2000; published 31 January 2001)

The clustering process of gold atoms in ion-implanted silica, during annealing in different atmospheres, is experimentally investigated and phenomenologically described. With respect to inert (Ar) or reducing (H_2 -Ar) atmosphere, annealing in oxidizing (air) atmosphere is the most effective in promoting cluster formation above 700–800 °C due to a thermally activated correlated diffusion of gold atoms and excess oxygen molecules coming from the atmosphere.

DOI: 10.1103/PhysRevB.63.075409

PACS number(s): 68.55.Ln, 61.46.+w, 66.30.-h, 85.40.Ry

I. INTRODUCTION

Ion implantation is a suitable technique to obtain glass composite materials with enhanced third-order optical nonlinearity.^{1,2} Implantation conditions (energy and ion fluence, as well as substrate temperature) and post implantation annealings allow us to obtain tailored materials for different applications. We focused our interest in gold implantation in silica glasses for two reasons: (i) the low diffusivity³ of the implanted species in comparison to other ones, to silver for example, minimizes the role of diffusion controlled processes, which occur in post implantation thermal annealings and, consequently, (ii) the possibility of varying the size and density of nanoparticle distribution by means of the atmosphere in which post implantation annealings take place.

For this purpose, fused silica slides were implanted with gold ions at a fluence above the threshold for spontaneous colloid precipitation and at a suitable energy for obtaining a subsurface buried layer of precipitates. Moreover, the implanted samples were isochronally and isothermally annealed in different atmospheres: air, Ar, and H_2 -Ar. After annealing in air, the surface plasmon resonance (SPR) signal, due to cluster formation, becomes more and more evident, as temperature increases.⁴ The transmission electron microscopy (TEM) data, together with the data obtained by the fitting procedure of the optical absorption data in the frame of the Maxwell-Garnett effective medium theory, provide details of the corresponding particle size and size distribution variations. No significant, or, rather, no comparable increase of the SPR signal was observed after annealings in Ar or in H_2 -Ar atmosphere up to 900 °C. The different behavior exhibited by the samples when exposed to different annealing atmospheres suggests that the increase of the Au cluster radius during the annealing in air should not be correlated to a dependence of the cluster melting temperature on the radius⁵ but rather to a thermodynamic interaction between gold atoms and O_2 molecules diffusing into the silica matrix. The idea is that oxygen permeation in implanted silica glasses essentially favors the gold transport through a thermally activated correlated diffusion that, in the following, will be described in the framework of the thermodynamics of the irreversible processes by showing that the O_2 concentration

gradient favors gold atoms diffusion and precipitation. On the contrary, during the annealing in argon atmosphere, no thermodynamic interaction may obviously take place while hydrogen is most probably involved in the saturation of dangling bonds produced by the collisional events occurring during implantation.

II. EXPERIMENT

Fused silica (Type II, Heraeus) slides were implanted at room temperature with an Au^+ ion beam at the INFN-INFN Ion Implantation Laboratory of INFN-Legnaro National Laboratories. Implantations were performed at room temperature and the current densities were maintained lower than $2 \mu A/cm^2$. The implantation conditions, 190 keV energy and $3 \times 10^{16} Au^+/cm^2$ ion dose, were chosen to have, after annealing, a subsurface buried layer of Au nanoparticle precipitation of some tens of nm thick (the ion projected range is about 70 nm). Ion-implanted slides were then heat treated at different temperatures at constant time, 1 h, in air, or in a H_2 -Ar gas mixture, or in pure Ar. Optical absorption spectra for all the samples were collected with a CARY 5E UV-VIS-NIR dual beam spectrophotometer in the 200–800 nm wavelength range. Microstructural and microanalytical characterization was performed by TEM with a Philips CM30T operating at 300 kV, equipped with an EDAX energy-dispersive spectrometer at CNR-LAMEL Institute in Bologna.

III. RESULTS AND DISCUSSION

Figure 1 shows the optical absorption spectra of an Au-implanted sample for different annealing temperatures T_A in air, in comparison with those measured in the samples annealed in Ar atmosphere. In the case of air annealing, a clear enhancement of the surface plasmon resonance (SPR) near 530 nm due to Au clusters in the matrix is evidenced above 700–800 °C, indicating the onset of faster nanoparticles growth. On the contrary, a modest increase in the SPR intensity is exhibited by the samples annealed in Ar, even at a high temperature, with a growth rate as small as the one observed in the low-temperature regime (< 700 °C) during

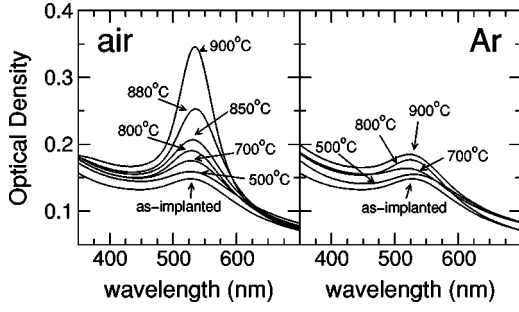


FIG. 1. Optical absorption spectra of Au-implanted silica samples at 3×10^{16} Au⁺/cm², 190 keV, annealed in air (left panel) or Ar (right panel) for 1 h at different temperatures.

air annealing. Results very similar to the Ar case have been obtained during H₂-Ar annealings.

In Fig. 2(a), the average cluster diameters, corresponding to samples annealed in air, are reported as a function of T_A . These values have been obtained either by TEM analysis (on the samples annealed at 400 °C, 700 °C, and 900 °C) or by fitting the optical absorption spectra in the frame of the Maxwell-Garnett effective medium theory, as follows. We consider a silica matrix containing N Au clusters in the volume V . The absorption coefficient α of the composite is defined through the Lambert-Beer absorption law: $I = I_0 e^{-\alpha x}$, where I_0 , I are the intensity before and after the sample of thickness x . If $f(R)$ is the normalized probability density of having a cluster radius R with photoabsorption cross-section $\sigma(R, \omega)$, the absorption coefficient $\alpha(\omega)$ can be written as

$$\alpha(\omega) = \frac{N}{V} \int_0^\infty dR f(R) \sigma(R, \omega). \quad (1)$$

Therefore, if we measure the optical density $OD(\omega)$ defined as

$$OD(\omega) = \log_{10} \left(\frac{I_0}{I} \right) = \log_{10}(e) \alpha(\omega) x, \quad (2)$$

we have

$$OD(\omega) = \log_{10}(e) x \frac{N}{V} \int_0^\infty dR f(R) \sigma(R, \omega). \quad (3)$$

For the calculation of the extinction cross-section $\sigma(R, \omega)$ we have used the Mie theory including multipolarity up to $l=3$ in order to account for retardation effects in the largest particles.⁶ The experimental bulk dielectric function used in the present study was taken from Ref. 7 and corrected for finite size.⁶ We have extracted through a nonlinear curve fit to the optical density the relevant parameters (average radius and standard deviation) of the $f(R)$. In the present case, $f(R)$ has been assumed to be a log-normal probability function that we verified to reproduce the size distribution experimentally observed by TEM in our samples. We have assessed the reliability of this procedure from the agreement of its results with those obtained by TEM, as can be seen in Fig. 3, which

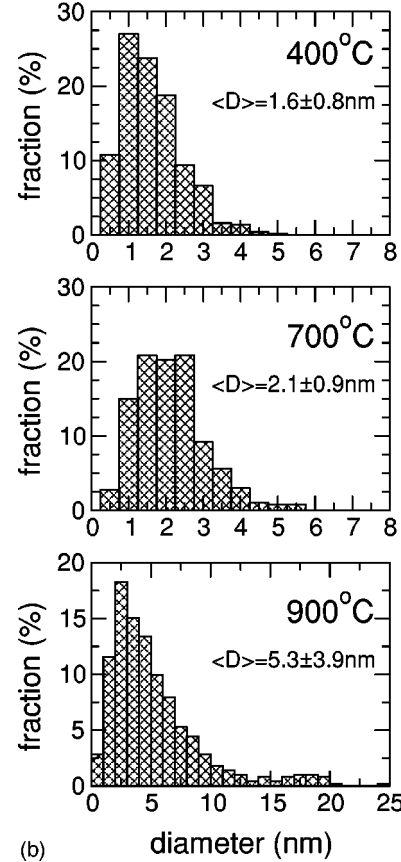
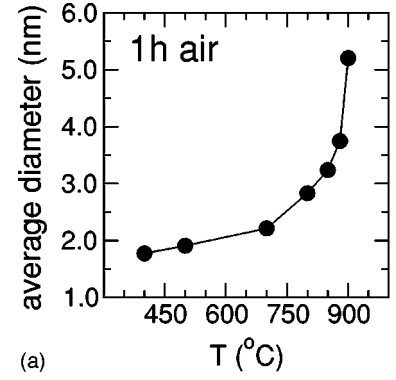


FIG. 2. (a) Average cluster diameter of Au-implanted silica samples at 3×10^{16} Au⁺/cm², 190 keV, annealed in air for 1 h at different temperatures; (b) corresponding histograms of the size distribution obtained by TEM analysis on the samples annealed at 400 °C, 700 °C, 900 °C.

reports the optical spectra of the air-annealed samples at 900 °C for 1 h along with the corresponding nonlinear fit obtained from Eq. (3).

The cluster size distributions for the TEM analyzed samples are also reported in Fig. 2(b). The progressive shift of the average cluster size towards higher values and the corresponding broadening of the cluster size distribution is evident. The results of TEM analysis give for the average cluster diameter $\langle D \rangle_{400^\circ\text{C}} = 1.6 \pm 0.8$ nm, $\langle D \rangle_{700^\circ\text{C}} = 2.1 \pm 0.9$ nm, $\langle D \rangle_{900^\circ\text{C}} = 5.3 \pm 3.9$ nm for the samples annealed in air at 400, 700, and 900 °C, respectively. Here, it is important to stress that for a fixed annealing time of 1 h, and by

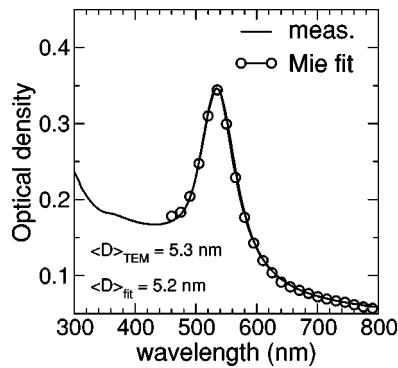


FIG. 3. Optical absorption spectra of Au-implanted silica sample at $3 \times 10^{16} \text{ Au}^+/\text{cm}^2$, 190 keV, annealed in air for one hour at 900°C (solid line). Empty circles represent the nonlinear fit to the experimental data, from which the average cluster diameter $\langle D \rangle_{fit}$ is obtained and compared to the TEM measured one, $\langle D \rangle_{TEM}$.

increasing temperature, the cluster size distribution increases, while clusters, having an average diameter as small as ~ 1 nm, are always observed. As we will see, this is a relevant point to establish the clusters growth mode that would be operating during the annealing process.

The evolution of cluster size with the temperature during air annealing can be seen in the TEM cross-sectional views of Fig. 4, where for comparison also the TEM micrograph of the Ar-annealed sample at 900°C is shown. Almost spherical Au clusters of different size are present in all the samples up to a depth of ~ 130 nm from the sample surface. Due to

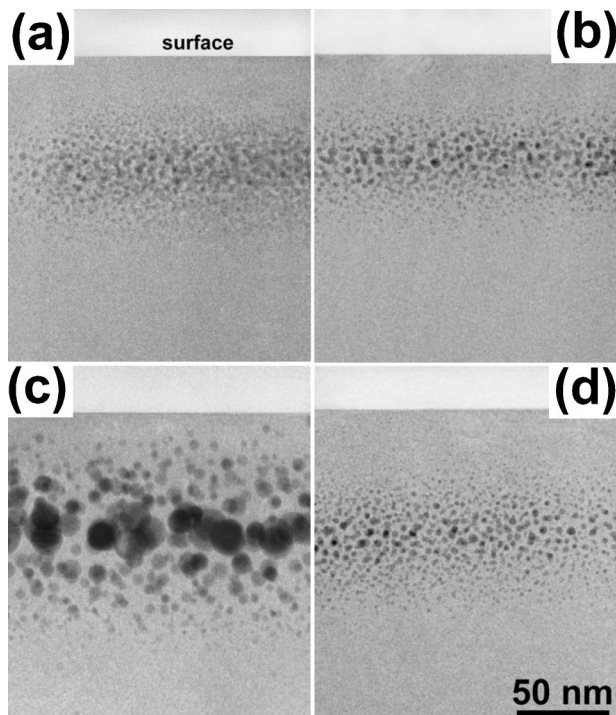


FIG. 4. Cross-sectional bright-field TEM views of Au-implanted silica samples at $3 \times 10^{16} \text{ Au}^+/\text{cm}^2$, 190 keV, annealed for one hour at: (a) 400°C in air, (b) 700°C in air, (c) 900°C in air, and (d) 900°C in Ar, respectively.

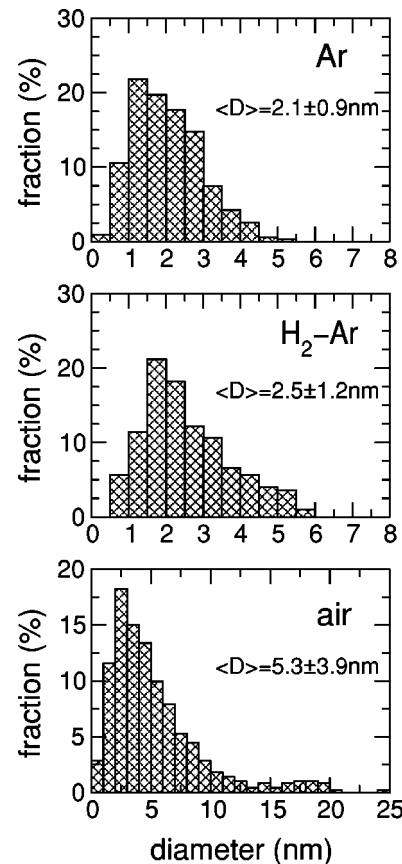


FIG. 5. TEM measured histograms of size distribution in the samples annealed 1 h at 900°C in different atmospheres: Ar (upper panel), H_2 -Ar (middle), and air (lower).

low gold diffusivity, the centroid of gold concentration does not move appreciably during the annealing and remains approximately near the implantation projected range (~ 70 nm), where, as the temperature increases, the largest clusters are formed.

The remarkable differences in the size distribution after annealing in the atmospheres presently investigated at 900°C for 1 h is sketched in Fig. 5: whereas Ar and H_2 -Ar annealing give comparable results ($\langle D \rangle = 2.1 \pm 0.9$ nm and $\langle D \rangle = 2.5 \pm 1.2$ nm, respectively), the sample annealed in air exhibits much larger and size-distributed clusters with $\langle D \rangle = 5.3 \pm 3.9$ nm. To better understand these results, we have analyzed them as a function of the temperature.

Figure 6 reports the Arrhenius plot of the squared average cluster radius after annealing in air or Ar, at a fixed time, 1 h. The corresponding data for the H_2 -Ar atmosphere are not reported, being very similar to the Ar case. The abrupt increase of cluster size, evidenced by Fig. 6 at about 800°C and also observed in the optical spectra intensity of Fig. 1(a) at the same temperature for air annealings, suggests that two different regimes for cluster growth occur during thermal treatments in air up to 900°C . Comparable results in Ag-implanted silica, after the air annealing process, are reported in Ref. 8.

To understand these two different regimes observed during annealing in air but neither in Ar nor in H_2 -Ar atmo-

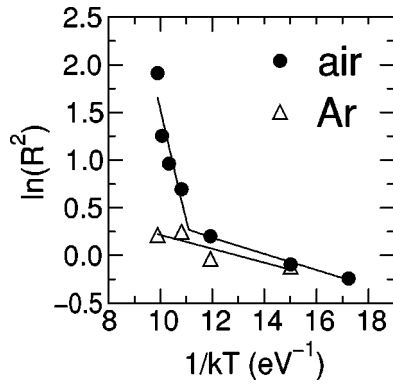


FIG. 6. Arrhenius plot of the squared average cluster radius R^2 after 1 h annealing in air (filled circles) or argon (empty triangles). Solid lines are linear fit to the experimental data.

spheres, it is necessary to look at the basic processes involved in gold diffusion and precipitation, in a silica matrix where Si-O bonds have been broken by ion implantation and oxygen deficiency point defects have been produced. Here, different diffusing species, namely oxygen or hydrogen or argon, may, or may not, interact both with the matrix and/or with the precipitating element, as well as with the above mentioned point defects, most probably E' defects.⁹

To do this, in the two following sections we will recall some basic features related to the kinetics of precipitation and then we will try to establish a general thermodynamic framework where the gold clustering process may be analyzed in terms of correlated diffusion parameters.

A. Some general remarks on precipitation processes

The precipitation process, in a supersaturated metastable alloy, which leads to the formation of large particles (i.e., particles with radii exceeding the critical radius) generally occurs by following three different stages. In the first stage, nuclei of the precipitating phase are formed with an average radius equal to the critical value. Here, homogeneous or heterogeneous nucleation may occur but in an ion-implanted system, where defects are produced, it is likely that just the produced defects may act as nucleating centers (heterogeneous nucleation). In the second stage, diffusional growth of the cluster occurs by solute depletion of the surrounding matrix without competing with the growth of any other particles. Here the growth is governed by the diffusion coefficient of the precipitating element and, more specifically, the average radius of the particle scales as $(Dt)^{1/2}$ where D is the diffusion coefficient and t is the diffusional time.^{10,11} In the third stage, the coarsening regime, the particle distribution established during the nucleation and growth period coarsens by the growth of larger particles. Here, the average radius of the growing particle scales as $(Dt)^{1/3}$.¹² The coarsening stage (also termed Ostwald ripening if the whole process occurs under mass conservation conditions) is governed by the Gibbs-Thomson effect where the chemical potential of a cluster is inversely proportional to the cluster size. This means that for a system containing both large and small clusters, the chemical potential difference causes material to be

transferred from small to large clusters: for this reason the diffusion coefficient D again controls the growth process.

Before concluding this section, we have to note that the distinction between a diffusional growth stage and a coarsening stage is somewhat arbitrary. In fact, it is only made in order to mark two special periods in the entire course of precipitation during which certain approximations can be made that allow, together with realistic boundary conditions for the concentration field, the rather complex diffusion problem to be solved analytically. However, the narrowing of the cluster size distribution starting from an initial configuration of precipitated particles, may be advocated as a signature of the Ostwald ripening.¹³ Finally, the scaling law of the cluster average radius with the kinetic Dt parameter suggests that to favor narrowing of the cluster size distribution (Ostwald ripening) one may perform isothermal annealing for different interval times or, for a fixed time, one may increase temperature to rise D . Obviously, to make a significant comparison, isothermal annealing at a different interval time, or increasing temperature, should not induce structural modification of the matrix into which clustering occurs.

B. Clustering of Au atoms

Having in mind the remarks of the previous section, an inspection of Fig. 2(b) clearly suggests that the observed clusters growth is controlled by atoms diffusion during the second stage of the precipitation process. Indeed, an increase of the cluster size distribution is observed as temperature increases while clusters, having an average radius as small as ~ 1 nm, are present both at 400 °C and 900 °C. The appearance of a small fraction, 1–2%, of clusters having an average large radius of 15–20 nm, when annealing is performed at 900 °C, further support the point that the Ostwald ripening should occur, at such a high temperature, for time exceeding 1 h. This point is also corroborated by our experimental results, where we studied gold cluster growth as a function of time at 900 °C. After 12 h annealing time, the bimodal distribution of the clusters size (with two main peaks at 10 nm and 25 nm—not reported here) is even more evident.

Having established that the clustering process we are analyzing is connected to a supersaturation of the precipitating element, then the meaning of the activation energy established by the Arrhenius plot of Fig. 6 is related to the height of the potential barrier, to be overcome in atomic jumping, as included in the diffusion coefficient. We will further comment on this point in the subsequent section.

However, when considering diffusion in implanted solids, the role of the produced point defects cannot be overlooked in agreement with the well-established framework of the radiation enhanced diffusion in solids where point defects, produced by the ion beam, exceed the equilibrium concentration.¹⁴ In the present case, point defects, most probably E' centers, are annealed at a temperature well below⁹ the temperature range 750–900 °C where the growth of the Au clusters is seen to increase significantly. This means that E' centers do not contribute to diffusion but they possibly may act as nucleation centers (heterogeneous nucleation) for gold clusters during the first stage of precipitation that occurs during implantation.

When looking at Fig. 6, a first point to be addressed concerns the charge state of gold. In other words, is there any connection between the different position of the knee in the Arrhenius plot and the different compensating charge effects when annealing occurs in air, or in argon, or in hydrogen-argon atmosphere? The answer is no for three different reasons. The first one comes from a simple estimation of the number of charges necessary to establish an electric field of 10^7 V/cm, thus inducing the dielectric breakdown: this is of the order of 10^{13} ions. This means that essentially all the implanted ions are neutralized during the implantation process as already reported in similar works.¹⁵ On the other hand, annealing in hydrogen atmosphere does not favor the Au mobility as it would be appropriate if a reduction mechanism would occur for a charged species. Moreover, an oxidation mechanism, which would occur when annealing is performed in air, should hinder the Au mobility, but just the annealing in air favors the Au clustering. In conclusion, from all the above considerations, the different temperature regimes observed for the Au clustering during annealing in different atmospheres are not connected with the charge state of the implanted Au that therefore may be safely assumed to be Au^0 . From Fig. 6, we observe that below 700–800 °C the cluster radius increases very slowly with the annealing temperature, at constant time, independently from the atmosphere composition. This very modest temperature dependence suggests a diffusion mechanism controlled by radiation damage.^{14,16,17} The measured activation energy of 1.17 eV/atom for gold diffusion in silica during annealing in air, in the temperature range from 750 to 900 °C, is very different from the literature value of 2.14 eV/atom.³ Note, however, that the activation energy for the molecular oxygen diffusion mechanism through an interstitial mechanism is in the range from 1.1 to 1.3 eV/atom.^{18,19} Considering that the clustering process is associated with gold diffusion, we have to understand why annealing in air may favor the precipitation of the metallic element. As a first guess, we may suppose that heating in air may favor, through oxygen migration coming from the ambient atmosphere, the annealing of radiation induced defects in silica mainly connected to the Si-O bond breaking with oxygen atoms displaced from their equilibrium lattice position. From this point of view we expect that gold diffusion could be enhanced in a recovered matrix. However, this seems not the case, because during implantation there is not preferential loss of oxygen from the silica matrix as proved by calculation with the TRIM software^{20,21} and so the global stoichiometry of the implanted silica is essentially preserved: this means that the oxygen atoms necessary to recover the silica matrix damage are already present in the gold-implanted silica. This point is consistent with the annealing mechanism of the E' centers as envisaged by Griscom⁹ and we further underline that such an annealing, which involves oxygen migration (most probably interstitial O_2 molecules), occurs in a temperature range⁹ well below the one we are analyzing, 750–900 °C for Au clustering. In conclusion, there is no apparent connection between the present diffusional growth stage of Au clusters and point defects annealing that possibly involves matrix recovering.

Nevertheless, the low Au diffusivity is evidenced in Ar and H_2 -Ar annealing atmospheres and also in a temperature regime higher than 800 °C, where the matrix recovery has been certainly completed:²² moreover, Rutherford backscattering spectrometry did not evidence an appreciable modification in the gold concentration profiles. Therefore, to explain the role of oxygen, coming from the ambient atmosphere, in promoting gold diffusivity, we may suggest that there is a thermodynamic interaction between oxygen and gold. In the framework of the thermodynamics of an irreversible process one may say that the chemical potential of oxygen in the silica matrix depends on both the matrix, as well as, the gold concentration. If gold and excess oxygen (i.e., oxygen coming from the external ambient) concentrations may be considered as dilute in the SiO_2 matrix, then the Kirkendall effect may be neglected in the oxygen and gold diffusion process and the atomic fluxes may be written in the linear response regime and, to better clarify the argument, in one-dimensional form, as follows:

$$J_i = -\frac{L_{ii}}{T} \frac{d(\mu_i - \mu_R)}{dx} - \frac{L_{i\gamma}}{T} \frac{d(\mu_\gamma - \mu_R)}{dx} \quad (4)$$

$$J_\gamma = -\frac{L_{\gamma i}}{T} \frac{d(\mu_i - \mu_R)}{dx} - \frac{L_{\gamma\gamma}}{T} \frac{d(\mu_\gamma - \mu_R)}{dx},$$

where i and γ stand for O_2 and Au^0 , respectively. The L 's are the Kelvin-Onsager phenomenological coefficients relating fluxes and forces, μ_R is the chemical potential of the SiO_2 matrix, and T is the silica matrix temperature. By using the Gibbs-Duhem relation, the quantity μ_R may be eliminated in Eqs. (4). Moreover, since in our approach, the analyzed system depends only on two independent variables n_i and n_γ the chemical potential of excess oxygen and gold may be written as

$$\mu_i = \mu_i(n_i, n_\gamma), \quad (5)$$

$$\mu_\gamma = \mu_\gamma(n_i, n_\gamma),$$

and therefore

$$\frac{d\mu_i}{dx} = \frac{\partial \mu_i}{\partial n_i} \frac{dn_i}{dx} + \frac{\partial \mu_i}{\partial n_\gamma} \frac{dn_\gamma}{dx}. \quad (6)$$

A similar expression holds for $d\mu_\gamma/dx$. By using these relations in Eqs. (4), after derivation and appropriate arrangement of the terms, we can write the fluxes J in a form analogous to Fick's first law. Finally, the continuity equations for the excess O_2 and Au atomic concentration are

$$\frac{\partial n_i}{\partial t} = D_{ii} \frac{\partial^2 n_i}{\partial x^2} + D_{i\gamma} \frac{\partial^2 n_\gamma}{\partial x^2}, \quad (7)$$

$$\frac{\partial n_\gamma}{\partial t} = D_{\gamma\gamma} \frac{\partial^2 n_\gamma}{\partial x^2} + D_{\gamma i} \frac{\partial^2 n_i}{\partial x^2},$$

where D 's are the ‘‘diffusion coefficients’’ that are considered independent of concentration (dilute impurity limit). Before examining our present problem of gold clustering in

the presence of excess oxygen transport, it is appropriate to underline that Eqs. (7) are very general thermodynamic equations that describe transport when diffusing species interact. From Eqs. (7), the movement of the element i also depends on the concentration gradient of element γ , and vice versa. Very clear evidence of such a thermodynamic interaction is reported, for example, in Fe-C-Si and in the Fe-C-Mn system, where Si enhances the C activity, while Mn hinders it.²³ More recently, epitaxial recrystallization of Li- or Cs-implanted α -SiO₂ was observed to be activated by annealing in oxygen atmosphere, with authors suggesting a correlation between oxygen, coming from the external atmosphere, and the alkali metals.²⁴

After establishing the general equations to analyze transport, when thermodynamic interaction occurs, let us now analyze the data reported in Fig. 6. The continuity equation governing excess oxygen concentration cannot be utilized here because we do not have any experimental information concerning the permeation oxygen profile. However, a permeating element should have a concentration profile with maximum located at the surface and going monotonically to zero at the interior of the absorbing matrix. Considering now the continuity equation governing the Au⁰ transport we see that, even if the $D\gamma\gamma$ coefficient is small in a low-medium temperature regime (700–900 °C) the $D\gamma i$ coefficient may have significant values in the same interval temperature: this implies that just the movement of the permeating oxygen drives the Au⁰ diffusion. In other words, the diffusion-controlled precipitation process of the metallic element is induced by the oxygen flux through the correlation coefficient $D\gamma i$. It is not possible to compare the activation energy of the thermodynamic correlation coefficient $D\gamma i$ with literature data because of the general lack of information in the field of correlation coefficients. However, since the diffusion of the permeating oxygen drives the gold movement, it is not surprising to obtain a $D\gamma i$ coefficient governed by an activation energy quite similar to the one of the interstitially diffusing O₂ molecule.

A major point now enters when reconsidering the meaning we have attributed to the data reported in Fig. 6: we said indeed that the square of the gold cluster radius is a linear function of the gold diffusion coefficient. This relation stems from modeling the clustering process by considering a balance between atoms joining the surface of a cluster whose radius exceeds the critical one, and atoms leaving the surface itself. The atomic flux coming from the supersaturated region around the growing cluster is then linearized and the final

equation that controls the cluster growth includes time constant parameters such as the supersaturation concentration of the precipitating element and the equilibrium concentration that is generally a vanishing quantity.^{10,11} In our new picture of the precipitation process, driven by the motion of the permeating oxygen molecules, the flux of the clustering element is not controlled by gold concentration but by an excess oxygen gradient. Following the linearization procedure adopted in Refs. 10 and 11, to obtain the time dependent cluster radius $R(t)$ we are able to write here a simplified closed expression for $R(t)$ that now includes an effective oxygen concentration term. However, the relevant point is that the Arrhenius plot of $R^2(t)$ still gives the activation energy of the diffusion coefficient that now is the correlation parameter $D\gamma i$.

IV. CONCLUSIONS

We have addressed the clustering problem of gold atoms implanted in silica glasses, following different annealing atmospheres, namely air, Ar or H₂-Ar. The cluster size distribution and the average cluster size have been determined by TEM. When including the square of the average cluster radius in an Arrhenius plot, two different regimes are evidenced when annealing occurs in air. To explain why, in the higher temperature regime, 750–900 °C, when point defects are certainly annealed, the clustering of gold atoms is favored during annealing in air, we have elaborated on a general model for gold atom diffusion interacting with excess oxygen coming from the external ambient. The clustering regime characterized by an activation energy of 1.17 eV/atom, very different from that appropriate to gold diffusion in silica (2.14 eV/atom) is then attributed to the thermodynamic correlation coefficient $D\gamma i$ in Eqs. (7). We plan to extend the analysis of the gold clustering problem for annealing in air at an interval time exceeding 1 h, when Ostwald ripening becomes most probably the relevant cluster growth mechanism.

ACKNOWLEDGMENTS

The technical assistance of M. Parolin and U. Pieri at INFN-INFM Ion Implantation Laboratory-Legnaro is gratefully acknowledged. This work has been partially supported by MURST (University and Research Ministry) within a National University Research Project and CNR within national Progetto Finalizzato MSTA II.

*Corresponding author: Email address: mattei@padova.infm.it

¹P. Mazzoldi, G.W. Arnold, G. Battaglin, F. Gonella, and R.F. Haglund, Jr., *J. Nonlinear Opt. Phys. Mater.* **5**, 285 (1996).

²F. Gonella and P. Mazzoldi, in *Handbook of Nanostructured Materials and Nanotechnology*, edited by H. S. Nalwa (Academic Press, San Diego, 1989), Vol. 4, pp. 81–158.

³D.R. Collins, D.K. Schroder, and C.T. Sah, *Appl. Phys. Lett.* **8**, 323 (1996).

⁴G.W. Arnold and J.A. Borders, *J. Appl. Phys.* **48**, 1488 (1977).

⁵P. Buffat and J.-P. Borel, *Phys. Rev. A* **13**, 2287 (1976).

⁶U. Kreibig and M. Vollmer, *Optical Properties of Metal Clusters* (Springer-Verlag, Berlin, 1995).

⁷P.B. Johnson and R.W. Christy, *Phys. Rev. B* **6**, 4370 (1972).

⁸D. Ila, E.K. Williams, S. Sarkisov, C.C. Smith, D.B. Poker, and D.K. Hensley, *Nucl. Instrum. Methods Phys. Res. B* **141**, 289 (1998).

⁹D.L. Griscom, *Nucl. Instrum. Methods Phys. Res. B* **1**, 481 (1984).

¹⁰H.B. Aaron, D. Fainstein, and G.R. Kotler, *J. Appl. Phys.* **41**, 4404 (1970).

- ¹¹A. Miotello, G. De Marchi, G. Mattei, P. Mazzoldi, and A. Quaranta, *Appl. Phys. A: Mater. Sci. Process.* **70**, 415 (2000).
- ¹²I.M. Lifshitz and V.V. Slezov, *Zh. Éksp. Teor. Fiz.* **35**, 479 (1958) [*Sov. Phys. JETP* **35**, 331 (1959)].
- ¹³G.R. Carlow, *Physica A* **239**, 65 (1997).
- ¹⁴G.J. Dienes and A.C. Damask, *J. Appl. Phys.* **29**, 1713 (1958).
- ¹⁵A.L. Stepanov, D.E. Hole, and P. Townsend, *J. Non-Cryst. Solids* **260**, 65 (1999).
- ¹⁶G. Battaglin, G. Della Mea, G. De Marchi, P. Mazzoldi, and A. Miotello, *Nucl. Instrum. Methods Phys. Res. B* **78**, 517 (1985).
- ¹⁷G. Arnold, G. Battaglin, G. Della Mea, G. De Marchi, P. Mazzoldi, and A. Miotello, *Nucl. Instrum. Methods Phys. Res. B* **32**, 315 (1988).
- ¹⁸M.A. Lamkin, F.L. Riley, and R.J. Fordham, *J. Eur. Ceram. Soc.* **10**, 347 (1992).
- ¹⁹F.J. Norton, *Nature (London)* **191**, 701 (1961).
- ²⁰J.P. Biersack and L.G. Haggmark, *Nucl. Instrum. Methods Phys. Res. B* **174**, 257 (1980).
- ²¹J. F. Ziegler, J. P. Biersack, and U. Littmark, in *The Stopping and Range of Ions in Solids*, edited by J. F. Ziegler (Pergamon, New York, 1985).
- ²²R.A.B. Devine, *Nucl. Instrum. Methods Phys. Res. B* **91**, 378 (1994).
- ²³L.S. Darken, *Trans. AIME* **180**, 430 (1949).
- ²⁴M. Gustafsson, F. Roccaforte, J. Keinonen, W. Bolse, L. Ziegeler, and K.P. Lieb, *Phys. Rev. B* **61**, 3327 (2000).